International Journal of Solids and Structures 48 (2011) 249–256

Contents lists available at ScienceDirect

International Journal of Solids and Structures

journal homepage: www.elsevier.com/locate/ijsolstr

Flexoelectric properties of ferroelectrics and the nanoindentation size-effect

M. Gharbi [a], Z.H. Sun [a], P. Sharma [a,b,*], K. White [a], S. El-Borgi [c]

[a] Department of Mechanical Engineering, University of Houston, Houston, TX 77204, USA
[b] Department of Physics, University of Houston, Houston, TX 77204, USA
[c] Ecole Polytechnique de Tunisie, Tunisia

ARTICLE INFO

Article history:
Received 30 May 2010
Received in revised form 17 September 2010
Available online 1 October 2010

Keywords:
Ferroelectrics
Flexoelectricity
Indentation

ABSTRACT

Recent works have established the critical role of flexoelectricity in a variety of size-dependent physical phenomena related to ferroelectrics including giant piezoelectricity at the nanoscale, dead-layer effect in nanocapacitors, dielectric properties of nanostructures among others. Flexoelectricity couples strain gradients to polarization in both ordinary and piezoelectric dielectrics. Relatively few experimental works exist that have determined flexoelectric properties and they all generally involve some sort of bending tests on micro-specimens. In this work, we present a straightforward method based on nanoindentation that allows the evaluation of flexoelectric properties in a facile manner. The key contribution is the development of an analytical model that, in conjunction with indentation load–displacement data, allows an estimate of the flexoelectric constants. In particular, we confirm the experimental results of other groups on $BaTiO_3$ which differ by three orders of magnitude from atomistic predictions. Our analytical model predicts (duly confirmed by our experiments) a strong indentation size-effect due to flexoelectricity.

1. Introduction

Piezoelectricity exists only in non-centrosymmetric crystals. However, a somewhat under-appreciated fact is that all dielectrics polarize when subjected to inhomogeneous strain. This phenomenon, the coupling of strain gradients to polarization, is known as flexoelectricity. Phenomenologically, the total polarization can be expressed as:

$$P_i = \underbrace{d_{ijk}\varepsilon_{jk}}_{=0,\ \text{for centrosymmetric materials}} + \mu_{ijkl}\frac{\partial \varepsilon_{jk}}{\partial x_l}. \quad (1)$$

Recently, flexoelectricity has generated much excitement due to the elucidation of several insights relevant at the nanoscale. For example, Catalan et al. (2004) have studied the impact of flexoelectricity on the dielectric properties and Curie temperature of ferroelectric materials while Cross and coworkers (1999, 2006) have proposed tantalizing notions such as "piezoelectric composites without using piezoelectric materials". Eliseev et al. (2009) have investigated the renormalization of properties of ferroelectric nanostructures due to the spontaneous flexoelectric effect as well as developed analytical approaches to derive size-effects in such nanostructures (Eliseev and Morozovska, 2009). One of us has demonstrated strong size-dependent enhancement of the apparent piezoelectric coefficient in materials that are intrinsically piezoelectric (Majdoub et al., 2008a, 2009b) as well as explored ramifications for energy harvesting (Majdoub et al., 2008b, 2009c). More recently Majdoub et al. (2009a) have also demonstrated, through first principles and theoretical calculations, that the so-called dead-layer effect in nanocapacitors may be strongly influenced by flexoelectricity. The reader is referred to reviews by Tagantsev (1986, 1991), Tagantsev et al. (2009) for further details.

Relatively few experimental works exists on the determination of flexoelectric properties of crystals. Cross and co-worker's pioneering work provided some of the first data on various perovskites like PMN, PZT, BST, and $BaTO_3$ (Ma and Cross, 2001, 2002, 2003, 2006; Fu et al., 2006, 2007). More, recently Zubko et al. (2007) have published the experimental characterization of the complete flexoelectric tensor for $SrTiO_3$. The afore-mentioned experimental approaches are predicated on bending experiments and are decidedly non-trivial. In parallel, various groups have also made atomistic predictions of flexoelectric properties. For example, one of us (Maranganti and Sharma, 2009) presented results for a number of dielectrics of technological and scientific interest. Dumitrica et al. (2002), Kalinin and Meunier (2008) discuss graphene and very recently, Hong et al. (2010) presented a first principles approach and consequent data for both $SrTiO_3$ and $BaTO_3$. While the theoretical works of various groups are all in agreement, the experimentally estimated flexoelectric constant of $BaTO_3$ is 3 orders of magnitude higher compared to the atomistically predicted value. The reasons for this discrepancy are still an open research issue (and beyond the scope of the present paper).

* Corresponding author at: Department of Mechanical Engineering, University of Houston, Houston, TX 77204, USA. Tel.: +1 281 723 4649.
E-mail address: psharma@uh.edu (P. Sharma).

0020-7683/$ - see front matter © 2010 Elsevier Ltd. All rights reserved.
doi:10.1016/j.ijsolstr.2010.09.021

In this paper, we present a nano-indentation based methodology to extract flexoelectricity properties of dielectrics. The key contribution is the development of an analytical model of indentation of a ferroelectric surface duly incorporating both piezoelectricity and flexoelectricity. This analytical model can then be used with rather easily generated load–displacement data to extract the desired properties. The outline of the paper is as follows: in Section 2, we present the mathematical problem followed by an approximate analytical solution. Experimental work is described in Section 3 and our major results are presented in Section 4. Implications of the present work, including the identification of the indentation size-effect due to flexoelectricity are discussed in Section 5 where we also summarize our conclusions. Some initial results on the indentation size-effects were communicated earlier by us in a rapid communication (Gharbi et al., 2009).

2. Indentation problem for piezoelectric-flexoelectric half-space

We consider the indentation of a transversely isotropic material by a circular flat indenter of radius a as shown in Fig. 1. Recently, Kalinin et al. (2004), Karapetian et al. (2005), have developed closed form solutions for piezoelectric half-space indentation problem for the cases of flat, spherical and conical indenters using the correspondence principle (Karapetian et al., 2002). The objective of this section is to present the mathematical development leading to expressions that inter-relate applied concentrated force P, concentrated charge Q, indentation depth w and tip potential ψ_0.

According to Majdoub et al. (2008a), the governing equations of a continuum with simultaneous presence of piezoelectricity and flexoelectricity valid for a dielectric occupying a volume V bounded by a surface S in a vacuum V' are:

$$\begin{aligned}
&\nabla\cdot\sigma+f=\rho\ddot{u} \text{ where } \sigma=c:S+d\cdot P+(e-f):\nabla P \text{ in } V,\\
&\overline{E}+\nabla\cdot\widetilde{E}-\nabla\varphi+E^0=0 \text{ in } V,\\
&-\varepsilon_0\Delta\varphi+\nabla\cdot P=0 \text{ in } V\\
&\Delta\varphi=0 \text{ in } V',
\end{aligned} \tag{2}$$

where

$$\begin{aligned}
&-\overline{E}=a\cdot P+g:\nabla P+f:\nabla\nabla u+d:S,\\
&\widetilde{E}=b:\nabla P+e:S+g\cdot P.
\end{aligned}$$

The second order tensor a is the reciprocal dielectric susceptibility and the fourth order tensor c is the elastic tensor. d and f are the third order piezoelectric tensor and the fourth order flexoelectric tensor respectively. The fourth order tensor b is the polarization gradient–polarization gradient coupling tensor. The fourth order tensor e corresponds to polarization gradient and strain coupling and g is the polarization-polarization gradient coupling tensor. For sake of simplicity, we note the term $(f-e)$ by f in the rest of our theoretical development.

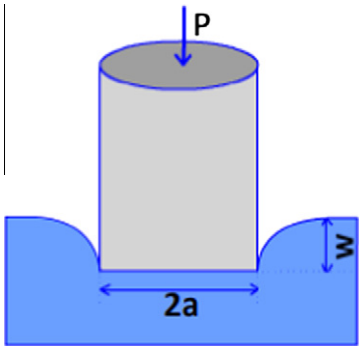

Fig. 1. Schematic of a transversely isotropic medium indented by circular flat indenter.

The corresponding boundary conditions are:

$$\begin{aligned}
&\sigma.n=t,\\
&\widetilde{E}.n=0,\\
&(-\varepsilon_0\|\varphi\|+P)\cdot n=0.
\end{aligned} \tag{3}$$

In anticipation of eventually applying perturbation theory to solve the rather complicated boundary value problem stated above, we define that for any $i,j=1,2,3,\ q=\frac{q_1}{a}=\frac{f_{ij}}{ad^*}$, where $\left(d^*=\frac{|d_{15}|+|d_{31}|+|d_{33}|}{3}\right)$. Then, constitutive equations for the case of transversely isotropic material may be explicitly written as follows:

$$\frac{\sigma_{ij}}{ad^*}=\frac{C_{ijkl}}{ad^*}S_{kl}+\varepsilon_0^{-1}\frac{d_{kij}}{ad^*}P_k-q\varepsilon_0^{-1}P_{l,k}, \tag{4}$$

$$\frac{D_i}{ad^*}=\frac{d_{ikl}}{ad^*}S_{kl}-\varepsilon_0^{-1}\frac{a_{ik}}{ad^*}P_k+qS_{kl,j}.$$

We re-write equilibrium equations $\partial\sigma_{ij}/\partial x_i=0$ and equation of electrostatics $\partial D_i/\partial x_i=0$ to obtain a system of four equations for displacements u_x,u_y,u_z and polarizations P_x, P_y andP_z.

$$\frac{C_{ijkl}}{ad^*}S_{kl,i}+\varepsilon_0^{-1}\frac{d_{kij}}{ad^*}P_{k,i}-q\varepsilon_0^{-1}P_{l,ki}=0, \tag{5}$$

$$\frac{d_{ikl}}{ad^*}S_{kl,i}-\varepsilon_0^{-1}\frac{a_{ik}}{ad^*}P_{k,i}+qS_{kl,ji}=0.$$

The remaining equation is:

$$P_{i,i}-\varepsilon_0\psi_{,ii}=0. \tag{6}$$

2.1. Solution of the problem for the case of circular flat indenter

The complexity of the above equations precludes an exact solution. We employ the perturbation approach, as (for example) used quite successfully by Holmes in a different context Holmes (1995).The present boundary value problem is a singular perturbation problem and accordingly, we separately present both "inner" and "outer" solutions.

2.1.1. Outer solution

The perturbation expansion is carried out in terms of the small parameter q.:

$$\begin{aligned}
&u_x^{outer}=u_x^0+o(q), \quad u_y^{outer}=u_y^0+o(q),\\
&u_z^{outer}=u_z^0+o(q), \quad P_x^{outer}=P_x^0+o(q),\\
&P_y^{outer}=P_y^0+o(q), \quad P_z^{outer}=P_z^0+o(q).
\end{aligned} \tag{7}$$

For purely mechanical problem (zero electrical conditions, $\psi=0$ for $(0\leqslant\rho\prec\infty)$ the boundary conditions are:

$$\begin{aligned}
&u_z^{outer}=w \text{ for } 0\leqslant\rho<a,\\
&\sigma_{zz}^{outer}=0 \text{ for } \rho>a,\\
&\tau_z^{outer}=0 \text{ for } 0\leqslant\rho<\infty.
\end{aligned} \tag{8}$$

For purely electrical problem (zero mechanical conditions, $u_z=0$ for $(0\leqslant\rho\prec\infty)$:

$$\begin{aligned}
&\psi^{outer}=\psi_0 \text{ for } 0\leqslant\rho<a,\\
&D_z^{outer}=0 \text{ for } \rho\succ a.
\end{aligned} \tag{9}$$

Inserting (7) into (5) and considering the leading order terms only, we obtain the outer system of equations. This corresponds to $q=0$ (absence of flexoelectricity)—i.e., the case of a purely piezoelectric material solved exactly by Karapetian et al. (2005). For the sake of completeness, Karapetian et. al.'s solution is summarized in

Appendix A. Therefore, the displacements and potential have the expressions given in (A.10) and (A.12). In addition, analogies between the outer system and (A.1.2) lead to the following relationships between the electric potential and polarizations:

$$P_x^{outer} = \varepsilon_0 \frac{\partial \psi^{outer}}{\partial x}, \quad P_y^{outer} = \varepsilon_0 \frac{\partial \psi^{outer}}{\partial y}, \quad P_z^{outer} = \varepsilon_0 \frac{\partial \psi^{outer}}{\partial z}. \tag{10}$$

2.1.2. Inner solution

In this section, we derive the solution for the inner problem. As a first step, we transform system (5) into cylindrical coordinates and consider the transition-layer coordinates:

$$\xi \equiv \frac{\frac{\rho}{a} - 1}{q} = \frac{\rho - a}{q_1}, \quad z \equiv z$$

After performing the previous transformations, the leading order for the new system yields the following set of equations:

$$\begin{aligned}
&\left(C_{11}\cos^2(\phi) + C_{66}\sin^2(\phi)\right)\frac{\partial^2(u_x^{inner})}{\partial \xi^2} \\
&\quad + (C_{11} - C_{66})\cos(\phi)\sin(\phi)\frac{\partial^2\left(u_y^{inner}\right)}{\partial \xi^2} \\
&\quad - d^*\cos(\phi)\frac{\partial^3 \psi^{inner}}{\partial \xi^3} = 0, \\
&(C_{11} - C_{66})\cos(\phi)\sin(\phi)\frac{\partial^2(u_x^{inner})}{\partial \xi^2} \\
&\quad + \left(C_{11}\sin^2(\phi) + C_{66}\cos^2(\phi)\right)\frac{\partial^2(u_y^{inner})}{\partial \xi^2} \\
&\quad - d^*\sin(\phi)\frac{\partial^3 \psi^{inner}}{\partial \xi^3} = 0, \\
&C_{44}\frac{\partial^2(u_z^{inner})}{\partial \xi^2} + d_{15}\frac{\partial^2 \psi^{inner}}{\partial \xi^2} = 0, \\
&d^*\cos(\phi)\frac{\partial^3(u_x^{inner})}{\partial \xi^3} + d^*\sin(\phi)\frac{\partial^3(u_y^{inner})}{\partial \xi^3} + d_{15}\frac{\partial^2(u_z^{inner})}{\partial \xi^2} \\
&\quad - a_{11}\frac{\partial^2 \psi^{inner}}{\partial \xi^2} = 0.
\end{aligned} \tag{11}$$

The boundary conditions used to solve the inner problem on plane $z = 0$ are:

For the purely mechanical problem:

$$\begin{aligned}
&u_z^{inner}(\xi, 0) = w \text{ for } -\infty < \xi < 0, \\
&\tau_z^{inner}(\xi, 0) = 0 \text{ for } -\infty < \xi < \infty, \\
&\sigma_{zz}^{inner}(\xi, 0) = 0 \text{ for } 0 < \xi < \infty, \\
&\psi^{inner}(\xi, 0) = 0 \text{ for } -\infty < \xi < 0.
\end{aligned} \tag{12}$$

For the purely electrical problem:

$$\begin{aligned}
&\psi^{inner}(\xi, 0) = \psi_0 \text{ for } -\infty < \xi < 0, \\
&u_z^{inner}(\xi, 0) = 0 \text{ for } -\infty < \xi < 0, \\
&D_z^{inner}(\xi, 0) = 0 \text{ for } 0 < \xi < \infty.
\end{aligned} \tag{13}$$

The matching conditions interrelating outer and inner problems and necessary to obtain the inner solution are:

$$\begin{aligned}
&\lim_{|\xi|\to\infty}\left(u_x^{inner}\right) = \lim_{\rho\to a}\left(u_x^{outer}\right), \\
&\lim_{|\xi|\to\infty}\left(u_y^{inner}\right) = \lim_{\rho\to a}\left(u_y^{outer}\right), \\
&\lim_{|\xi|\to\infty}\left(u_z^{inner}\right) = \lim_{\rho\to a}\left(u_z^{outer}\right), \\
&\lim_{|\xi|\to\infty}\left(\psi^{inner}\right) = \lim_{\rho\to a}\left(\psi^{outer}\right).
\end{aligned} \tag{14}$$

Solving these set of equations for $-\infty < \xi < \infty$ and verifying both boundary conditions and matching conditions for u_x, u_y, u_z and ψ, we obtain expressions (B.1) and (B.2) for the inner potential and displacements (see Appendix B).

2.1.3. The entire solution

Now, according to perturbation approach outlined by Holmes (1995), we determine the entire solution for displacements u_x, u_y, u_z and potential ψ as follows:

For the purely mechanical problem:

$$\begin{aligned}
u_x &= -\cos(\phi)\frac{2wH^*}{\pi}\sum_{j=1}^{3}\left[N_j^*C_1^* + L_j^*C_2^*\right]\frac{a}{\rho}\left[1 - \frac{(a^2 - l_{1j}^2)^{1/2}}{a}\right] \\
&\quad + sign(a-\rho)\frac{w}{\pi^2 a}F_1(z)\cos(\phi)\sqrt{\frac{\left(C_{44}a_{11} + d_{15}^2\right)}{C_{11}C_{44}}}e^{-A^i\left|\frac{\rho-a}{q_1}\right|}, \\
u_y &= -\sin(\phi)\frac{2wH^*}{\pi}\sum_{j=1}^{3}\left[N_j^*C_1^* + L_j^*C_2^*\right]\frac{a}{\rho}\left[1 - \frac{(a^2 - l_{1j}^2)^{1/2}}{a}\right] \\
&\quad + sign(a-\rho)\frac{w}{\pi^2 a}F_1(z)\sin(\phi)\sqrt{\frac{\left(C_{44}a_{11} + d_{15}^2\right)}{C_{11}C_{44}}}e^{-A^i\left|\frac{\rho-a}{q_1}\right|},
\end{aligned} \tag{15}$$

$$\begin{aligned}
u_z &= -\frac{2wH^*}{\pi}\sum_{j=1}^{3}\frac{m_j^*}{\gamma_j^*}\left[N_j^*C_1^* + L_j^*C_2^*\right]\arcsin\left(\frac{a}{l_{2j}}\right) \\
&\quad - \frac{w}{\pi^2 a}\frac{d_{15}}{C_{44}}F_1(z)e^{-A^i\left|\frac{\rho-a}{q_1}\right|},
\end{aligned}$$

$$\psi = -\frac{2wH^*}{\pi}\sum_{j=1}^{3}\frac{k_j^*}{\gamma_j^*}\left[N_j^*C_1^* + L_j^*C_2^*\right]\arcsin\left(\frac{a}{l_{2j}}\right) + \frac{w}{\pi^2 a}F_1(z)e^{-A^i\left|\frac{\rho-a}{q_1}\right|}.$$

For the purely electrical problem:

$$\begin{aligned}
u_x &= -\cos(\phi)\frac{2\psi_0 H^*}{\pi}\sum_{j=1}^{3}\left[N_j^*C_3^* + L_j^*C_4^*\right]\frac{a}{\rho}\left[1 - \frac{\left(a^2 - l_{1j}^2\right)^{1/2}}{a}\right] \\
&\quad + sign(a-\rho)\cos(\phi)\frac{\psi_0}{\pi^2 a}F_6(z)\sqrt{\frac{\left(C_{44}a_{11} + d_{15}^2\right)}{C_{11}C_{44}}}e^{-A^i\left|\frac{\rho-a}{q_1}\right|}, \\
u_y &= -\sin(\phi)\frac{2\psi_0 H^*}{\pi}\sum_{j=1}^{3}\left[N_j^*C_3^* + L_j^*C_4^*\right]\frac{a}{\rho}\left[1 - \frac{\left(a^2 - l_{1j}^2\right)^{1/2}}{a}\right] \\
&\quad + sign(a-\rho)\sin(\phi)\frac{\psi_0}{\pi^2 a}F_6(z)\sqrt{\frac{\left(C_{44}a_{11} + d_{15}^2\right)}{C_{11}C_{44}}}e^{-A^i\left|\frac{\rho-a}{q_1}\right|},
\end{aligned} \tag{16}$$

$$\begin{aligned}
u_z &= -\frac{2\psi_0 H^*}{\pi}\sum_{j=1}^{3}\frac{m_j^*}{\gamma_j^*}\left[N_j^*C_3^* + L_j^*C_4^*\right]\arcsin\left(\frac{a}{l_{2j}}\right) \\
&\quad - \frac{\psi_0}{\pi^2 a}\frac{d_{15}}{C_{44}}F_6(z)e^{-A^i\left|\frac{\rho-a}{q_1}\right|},
\end{aligned}$$

$$\psi = -\frac{2\psi_0 H^*}{\pi}\sum_{j=1}^{3}\frac{k_j^*}{\gamma_j^*}\left[N_j^*C_3^* + L_j^*C_4^*\right]\arcsin\left(\frac{a}{l_{2j}}\right) + \frac{\psi_0}{\pi^2 a}F_6(z)e^{-A^i\left|\frac{\rho-a}{q_1}\right|}.$$

2.2. Stiffness relations

Stiffness relations describe relationships between applied force, P, and concentrated charge, Q, (required to maintain prescribed w and ψ_0) to w and $\psi_0 \cdot \sigma_{zz}$ and D_z may be written as:

$$\sigma_{zz} = \sigma^0_{zz} + q\sigma^1_{zz} \quad \text{and} \quad D_z = D^0_z + qD^1_z. \tag{17}$$

We assume that for small values of q:

$$\sigma_{zz} \approx \sigma^0_{zz} \quad \text{and} \quad D_z \approx D^0_z.$$

Then we obtain expressions of normal stresses and normal electric displacements for $\rho \prec a$ (contact zone) as follows:

For purely mechanical problem we find that σ^m_{zz} and D^m_z are:

$$\sigma^m_{zz} = -\frac{C^*_1 w}{\pi^2(a^2-\rho^2)^{1/2}} + \frac{f^*_1 w}{\pi^2 a} e^{A^i\left(\frac{\rho-a}{q_1}\right)} \quad \text{and}$$

$$D^m_z = \frac{C^*_2 w}{\pi^2(a^2-\rho^2)^{1/2}} - \frac{f^*_2 w}{\pi^2 a} e^{A^i\left(\frac{\rho-a}{q_1}\right)}, \tag{18}$$

where f^*_1 and f^*_2 are defined in Appendix C.

For purely mechanical problem we find that σ^e_{zz} and D^e_z are:

$$\sigma^e_{zz} = -\frac{C^*_3 \psi_0}{\pi^2(a^2-\rho^2)^{1/2}} + \frac{f^*_3 \psi_0}{\pi^2 a} e^{A^i\left(\frac{\rho-a}{q_1}\right)} \quad \text{and}$$

$$D^e_z = \frac{C^*_4 \psi_0}{\pi^2(a^2-\rho^2)^{1/2}} - \frac{f^*_4 w}{\pi^2 a} e^{A^i\left(\frac{\rho-a}{q_1}\right)}, \tag{19}$$

where f^*_3 and f^*_4 are defined in Appendix C.

Using (A.14), we obtain the new stiffness relations duly incorporating flexoelectricity:

$$P = \frac{2a}{\pi}\left(C^*_1 w + C^*_3 \psi_0\right) - \frac{2}{\pi a}\left(f^*_1 w + f^*_3 \psi_0\right) f_{q_1}(a), \tag{20.1}$$

$$Q = \frac{2a}{\pi}\left(C^*_1 w + C^*_3 \psi_0\right) - \frac{2}{\pi a}\left(f^*_2 w + f^*_4 \psi_0\right) f_{q_1}(a), \tag{20.2}$$

where $f_{q_1}(a)$ is defined as:

$$f_{q_1}(a) = \frac{q_1}{(A^i)^2}\left(q_1 e^{-\frac{A^i}{q_1}a} - q_1 + A^i a\right). \tag{21}$$

3. Indentation experiments

We set the potential $\psi_0 = 0$ in Eq. (20.1). In classical piezoelectricicty, the stiffness relation, for mechanical load, is then reduced to:

$$\frac{P}{a} = \frac{2}{\pi} C^*_1 w$$

Utilization of the Eq. (20.1) to determine the flexoelectric coefficient requires load–displacement data as a function of contact radius. We performed nanoindentation experiments on two materials. The first one is (001) oriented $BaTiO_3$ single crystal ($5 \times 5 \times 1$ mm) (Sun and White (2008)), and the second one is quartz single crystal (z-cut, $10 \times 10 \times 0.5$ mm)—both obtained from MTI Corporation, Richmond, CA. Quartz is expected to have negligible flexoelectricity (at least compared to $BaTiO_3$) and thus was chosen to provide a benchmark. A series of nanoindentations with a Berkovich indenter were performed on each sample using a commercial nanoindentation system with the continuous stiffness measurement (CSM) option (Nanoindenter XP, MTS Nano Instruments, Oak Ridge, TN). The indentation load was applied at a constant strain rate of 0.05 s^{-1} until the maximum displacement into surface was reached. By superimposing a small sinusoidal oscillation on the quasistatic primary loading force and analyzing the dynamic response of the indentation system, the CSM option allows a continuous measurement of contact stiffness during the entire loading, not just at the point of initial unloading as in the traditional measurement (Oliver and Pharr (1992), Hay and Pharr (2000)).

In the case of purely mechanical loading, it is shown in Karapetian et al. (2002) paper that for axisymmetric indenters (i.e., circular contacts) on transversely isotropic piezoelectric materials, the contact stiffness is independent of the indenter geometry and is given by,

$$s = 2\frac{C^*_1}{\pi} a$$

where C^*_1 is the indentation elastic stiffness for the piezoelectric indentation problem, and a is contact radius. The linear relation between contact stiffness and contact radius is identical to the case of indentation on elastically isotropic half spaces shown by Oliver and Pharr (1992) if we replace C^*_1 by πE_r, where E_r is the reduced elastic modulus. This stiffness relation was derived for an axisymmetric indenter (circular contacts), however, it has been shown that it works well even for the non-axisymmetric indenters (Oliver and Pharr (1992), Hay and Pharr (2000)). To obtain contact stiffness versus contact radius curve (s-a curve) for a circular flat indenter, various indenter radii should be used. However, considering the geometry-independent stiffness relation in the case of purely mechanical loading and with the CSM option of our nanoindentation system, the s-a curve for circular flat indenter can be experimentally obtained in one sample experiment with a conical or a pyramidal indenter. Since it is difficult to manufacture and maintain a conical indenter with a sharp tip, the reliable data in the small-scale cannot be readily obtained. Therefore, we adopted a sharp Berkovich indenter (three-sided pyramid, the tip radius ~50 nm) at the expense of well-defined contact radius. The area function of the indenter tip, $A = f(h_c)$ was carefully calibrated using the standard procedure, (Oliver and Pharr (1992), Hay and Pharr (2000)), where h_c is the contact depth. Although the projected contact area is not circular for the Berkovich indenter, the effective contact radius is calculated from the contact area by $\pi a^2 = f(h_c)$.

4. Results and discussions

The contact stiffness versus contact radius curves for $BaTiO_3$ and quartz are shown in Figs. 2 and 3, respectively. Fig. 2 illustrates experimental data $s = f(a)$ for both $BaTiO_3$ and quartz as well as what theoretical results based on pure piezoelectricity would predict (i.e., without flexoelectricity).

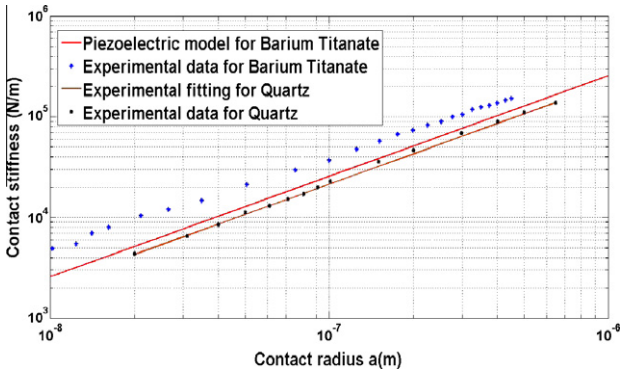

Fig. 2. Variation of the contact stiffness with respect to the contact radius a for $BaTiO_3$ and quartz (in logarithmic scale).

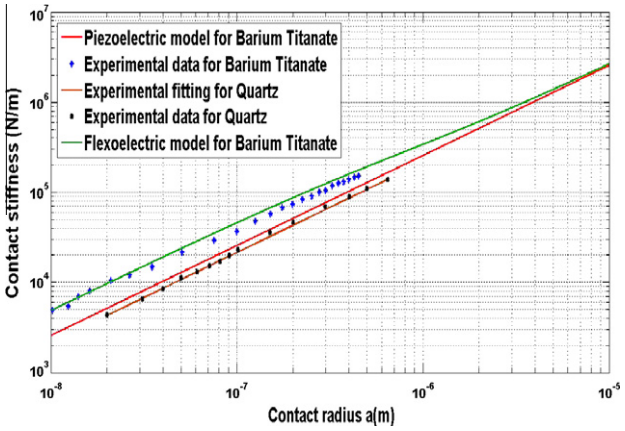

Fig. 3. Variation of the contact stiffness as a function of contact radius (in logarithmic scale). Experimental results for both $BaTiO_3$ and quartz are plotted along with the results from the fitted flexoelectric model and classical piezoelectricity based models.

According to Fig. 2, the contact stiffness vs. the indenter contact radius experimental curve exhibits a linear variation for the case of quartz. Consequently, we can conclude that quartz exhibits no size-effect and that classical piezoelectricity describes its behavior adequately. In other words, the order of magnitude of the flexoelectric coefficients for quartz is very low that no size effects can be observable (at least in the contact sizes investigated). On the other hand, it is clear that $BaTiO_3$ exhibits a marked size effect. The experimental results described by the blue dots shows a deviation with respect to the red line representing the classical piezoelectric model. Therefore the size-effect, in conjunction with Eq. (20.1) allows a determination of the flexoelectric constant. The parameter $q_1^{BaTiO_3}$ represents the ratio of the flexoelectric order of magnitude and the average piezoelectric coefficients. It is worthwhile to note that, the amount of deviation between flexoelectric and purely piezoelectric model essentially depends on $q_1^{BaTiO_3}$.

Fig. 3 shows that, for Barium Titanate, $q_1^{BaTiO_3} \approx 2 \times 10^{-7}$ m. It is important to note that our flexoelectric model exhibits the same variation as the piezoelectric model for contact radius bigger than 5 μm. Also, we note that for contact radius a smaller than 10^{-7} m ignoring higher order terms in Eq. (7) might affect our results (at that point, the assumptions of our perturbation theory may become questionable). However, since our results still correspond well with experimental data even for contact radii smaller than10^{-7} m, we tentatively conclude that even for q slightly larger than 1, our model remains valid—Further details about this issue are discussed by Holmes (1995, pp. 91–94) where in certain perturbation problems (despite expectations to the contrary) the approximate results emerge to be surprisingly correct. Our final estimate is $f_{12}^{BaTiO_3} \approx 4 \times 10^{-6}$ C/m which is in good agreement with experimental results, found by other groups using bending experiments (Cross, 2006).

The present work highlights two important aspects: (i) Flexoelectricity is the cause of a significant indentation size-effect in BaTiO3, (ii) indentation experiments may be used to provide estimates for flexoelectric behavior. Our approach may be further refined to provide information on multiple components of the flexoelectric tensor. A reasonable question to ask is whether dislocations (or perhaps domain nucleation or domain wall motion) are the cause of observed size-effect rather than flexoelectricity? We do not believe that dislocations play a major role in the observed size-effect. Both quartz and $BaTiO_3$ are expected to exhibit "similar" dislocation behavior however the latter (simply based on its high dielectric constant) is expected to have a much larger flexoelectric response). As evident, quartz showed negligible size-effect in the contact sizes investigated. The role of domain walls is trickier to unravel. The contact size is wholly located within a single domain however this does preclude new domains being nucleated. Therefore, it may be very well possible that the flexoelectric constant that we estimate contains both an intrinsic part as well an extrinsic part due to domain wall behavior (e.g. see, Damjanovic, 2005 and references therein for piezoelectric behavior). If that is the case, given the good agreement with bending experiments, the same must hold for the latter. Finally, having independently confirmed experimental results of other groups using a completely different approach, the discrepancy between experimental results and those of atomistic predictions can be considered to be definite—in other words, the discrepancy is not a peculiarity of experimental method or simulation approach and is intrinsic and remains a puzzle to this date.

Acknowledgements

The UH team was supported by NSF Grant CMMI 0826153. The international component of the work was supported by NIRT Grant No. CMMI 0708096 and IMI center IIMEC.

Appendix A

This Appendix summarizes the results of Karapetian et al. (2005) and their notation is retained. We consider transversely isotropic material property variation (for elastic constants (N/m^2), piezoelectric coupling (C/m^2) and dielectric permeabilities (F/m)). The linear constitutive equations have the following forms:

$$\begin{aligned}
\sigma_{xx} &= C_{11}\frac{\partial u_x}{\partial x} + (C_{11}-2C_{66})\frac{\partial u_y}{\partial y} + C_{13}\frac{\partial u_z}{\partial z} + d_{31}\frac{\partial \psi}{\partial z},\\
\sigma_{yy} &= (C_{11}-2C_{66})\frac{\partial u_x}{\partial x} + C_{11}\frac{\partial u_y}{\partial y} + C_{13}\frac{\partial u_z}{\partial z} + d_{31}\frac{\partial \psi}{\partial z},\\
\sigma_{zz} &= C_{13}\frac{\partial u_x}{\partial x} + C_{13}\frac{\partial u_y}{\partial y} + C_{33}\frac{\partial u_z}{\partial z} + d_{33}\frac{\partial \psi}{\partial z},\\
\sigma_{xy} &= C_{66}\left(\frac{\partial u_x}{\partial y} + \frac{\partial u_y}{\partial x}\right),\\
\sigma_{yz} &= C_{44}\left(\frac{\partial u_y}{\partial z} + \frac{\partial u_z}{\partial y}\right) + d_{15}\frac{\partial \psi}{\partial y},\\
\sigma_{zx} &= C_{44}\left(\frac{\partial u_x}{\partial z} + \frac{\partial u_z}{\partial x}\right) + d_{15}\frac{\partial \psi}{\partial x}.
\end{aligned} \tag{A.1.1}$$

For electric displacements:

$$D_x = d_{15}\left(\frac{\partial u_x}{\partial z} + \frac{\partial u_z}{\partial x}\right) - a_{11}\frac{\partial \psi}{\partial x},$$

$$D_y = d_{15}\left(\frac{\partial u_y}{\partial z} + \frac{\partial u_z}{\partial y}\right) - a_{11}\frac{\partial \psi}{\partial y},$$

$$D_z = d_{31}\left(\frac{\partial u_x}{\partial x} + \frac{\partial u_y}{\partial y}\right) + d_{33}\frac{\partial u_z}{\partial z} - a_{33}\frac{\partial \psi}{\partial z}.$$

We write equilibrium equations $\partial\sigma_{ij}/\partial x_i = 0$ and the equation of electrostatics $\partial D_i/\partial x_i = 0$ for transversely isotropic material as follows:

$$\begin{aligned}
&C_{11}\frac{\partial^2 u_x}{\partial x^2} + C_{66}\frac{\partial^2 u_x}{\partial y^2} + C_{44}\frac{\partial^2 u_x}{\partial z^2} + (C_{11}-C_{66})\frac{\partial^2 u_y}{\partial x \partial y}\\
&\quad + (C_{13}+C_{44})\frac{\partial^2 u_z}{\partial x \partial z} + (d_{31}+d_{15})\frac{\partial^2 \psi}{\partial x \partial z} = 0,
\end{aligned}$$

$$C_{66}\frac{\partial^2 u_y}{\partial x^2}+C_{11}\frac{\partial^2 u_y}{\partial y^2}+C_{44}\frac{\partial^2 u_y}{\partial z^2}+(C_{11}-C_{66})\frac{\partial^2 u_x}{\partial x\partial y}+(C_{13}+C_{44})\frac{\partial^2 u_z}{\partial y\partial z}+(d_{31}+d_{15})\frac{\partial^2 \psi}{\partial y\partial z}=0, \tag{A.1.2}$$

$$C_{44}\left(\frac{\partial^2 u_z}{\partial x^2}+\frac{\partial^2 u_z}{\partial y^2}\right)+C_{33}\frac{\partial^2 u_z}{\partial z^2}+(C_{44}+C_{13})\left(\frac{\partial^2 u_x}{\partial x\partial z}+\frac{\partial^2 u_y}{\partial y\partial z}\right)+d_{15}\left(\frac{\partial^2 \psi}{\partial x^2}+\frac{\partial^2 \psi}{\partial y^2}\right)+d_{33}\frac{\partial^2 \psi}{\partial z^2}=0,$$

$$d_{15}\left(\frac{\partial^2 u_z}{\partial x^2}+\frac{\partial^2 u_z}{\partial y^2}\right)+d_{33}\frac{\partial^2 u_z}{\partial z^2}+(d_{15}+d_{31})\left(\frac{\partial^2 u_x}{\partial x\partial z}+\frac{\partial^2 u_y}{\partial y\partial z}\right)-a_{11}\left(\frac{\partial^2 \psi}{\partial x^2}+\frac{\partial^2 \psi}{\partial y^2}\right)-a_{33}\frac{\partial^2 \psi}{\partial z^2}=0.$$

To solve the previous equilibrium equations, we introduce the following complex notations for displacements, u_i, stresses, σ_{ij}, electric potential ψ and electric displacements D_i

$$u\equiv u_x+iu_y,\quad u_z,\quad \psi,\quad D\equiv D_x+iD_y,\quad D_z,$$

$$\sigma_1\equiv\sigma_{xx}+\sigma_{yy},\quad \sigma_2\equiv\sigma_{xx}-\sigma_{yy}+2i\sigma_{xy},\quad \sigma_{zz},\quad \tau_z\equiv\sigma_{zx}+i\sigma_{yz}. \tag{A.2}$$

To simplify the understanding of the derivations we also introduce the following expressions:

$$\alpha_j^*=C_{44}\left(1+m_j^*\right)+d_{15}k_j^*,\quad \beta_j^*=d_{15}\left(1+m_j^*\right)-a_{11}k_j^*\quad (j=1,2,3). \tag{A.3}$$

Constants m_j^* and k_j^* are defined by the following relations ($j=1,2,3$):

$$m_j^*=\frac{\left(C_{11}\gamma_j^{*2}-C_{44}\right)\left(a_{33}-\gamma_j^{*2}a_{11}\right)+\gamma_j^{*2}(d_{15}+d_{31})^2}{\left(d_{33}-\gamma_j^{*2}d_{15}\right)(d_{15}+d_{31})+(C_{13}+C_{44})\left(a_{33}-\gamma_j^{*2}a_{11}\right)},$$
$$k_j^*=\frac{\left(C_{11}\gamma_j^{*2}-C_{44}\right)\left(d_{33}-\gamma_j^{*2}d_{15}\right)-\gamma_j^{*2}(d_{15}+d_{31})(C_{13}+C_{44})}{\left(d_{33}-\gamma_j^{*2}d_{15}\right)(d_{15}+d_{31})+(C_{13}+C_{44})\left(a_{33}-\gamma_j^{*2}a_{11}\right)}, \tag{A.4}$$

where $\gamma_j^{*2}=\lambda_j$ are roots of the following cubic equation:

$$A\lambda_j^3-B\lambda_j^2+C\lambda_j-D=0, \tag{A.5}$$

where A, B, C and D are defined as follows:

$$A=C_{11}\left(C_{44}a_{11}+d_{15}^2\right),$$
$$B=C_{44}\left[C_{11}a_{33}+(d_{15}+d_{31})^2\right]+a_{11}\left[C_{11}C_{33}+C_{44}^2-(C_{13}+C_{44})^2\right]+2d_{15}[C_{11}d_{33}-(C_{13}+C_{44})(d_{15}+d_{31})]+C_{44}d_{15}^2,$$
$$C=C_{33}[C_{44}a_{11}+(d_{15}+d_{31})^2]+a_{33}[C_{11}C_{33}+C_{44}^2-(C_{13}+C_{44})^2]+2d_{33}[C_{44}d_{15}-(C_{13}+C_{44})(d_{15}+d_{31})]+C_{11}d_{33}^2,$$
$$D=C_{44}\left(C_{33}a_{33}+d_{33}^2\right). \tag{A.6}$$

The results for (A.5) are:

$$\frac{C_{44}+m_j^*(C_{13}+C_{44})+k_j^*(d_{15}+d_{31})}{C_{11}}=\frac{m_j^*C_{33}+k_j^*d_{33}}{m_j^*C_{44}+(C_{13}+C_{44})+k_j^*d_{15}}=\frac{m_j^*d_{33}-k_j^*a_{33}}{m_j^*d_{15}+(d_{15}+d_{31})-k_j^*a_{11}}=\gamma_j^{*2}\equiv\lambda_j,\gamma_4^*=\sqrt{\frac{C_{44}}{C_{66}}}. \tag{A.7}$$

The following clusters of the piezoelectric constants are defined:

$$H^*=\frac{1}{2\pi\left(d_{15}^2+c_{44}a_{11}\right)\sum_{j=1}^{3}\left(\alpha_j^*a_j^*/\gamma_j^{*2}\right)}=-\frac{1}{2\pi\sum_{j=1}^{3}\alpha_j^*N_j^*},$$
$$N_1^*=\frac{\alpha_3^*\beta_2^*}{\gamma_3^*}-\frac{\alpha_2^*\beta_3^*}{\gamma_2^*},\quad L_1^*=\frac{\alpha_3^*\alpha_2^*}{\gamma_3^*}-\frac{\alpha_2^*\alpha_3^*}{\gamma_2^*},$$
$$a_1^*=\gamma_1^*\left[(1+m_2^*)k_3^*-(1+m_3^*)k_2^*\right],\quad 1\to2\to3\to1$$
and
$$C_1^*=-\frac{1}{B^*}\sum_{j=1}^{3}\frac{k_j^*}{\gamma_j^*}L_j^*,\quad C_2^*=\frac{1}{B^*}\sum_{j=1}^{3}\frac{k_j^*}{\gamma_j^*}N_j^*,$$
$$C_3^*=\frac{1}{B^*}\sum_{j=1}^{3}\frac{m_j^*}{\gamma_j^*}L_j^*,\quad C_4^*=-\frac{1}{B^*}\sum_{j=1}^{3}\frac{m_j^*}{\gamma_j^*}N_j^*,$$
$$B^*=H^*\left[\sum_{j=1}^{3}\frac{m_j^*}{\gamma_j^*}N_j^*\sum_{i=1}^{3}\frac{k_i^*}{\gamma_i^*}L_i^*-\sum_{j=1}^{3}\frac{m_j^*}{\gamma_j^*}L_j^*\sum_{i=1}^{3}\frac{k_i^*}{\gamma_i^*}N_i^*\right]. \tag{A.8}$$

Also, we define the following geometric relations ($j=1,2,3$):

$$2l_{1j}(z)=\sqrt{(a+\rho)^2+z_j^2}-\sqrt{(a-\rho)^2+z_j^2},$$
$$2l_{2j}(z)=\sqrt{(a+\rho)^2+z_j^2}+\sqrt{(a-\rho)^2+z_j^2}, \tag{A.9}$$
$$z_j=z/\gamma_j^*.$$

The solution of the system (A.1.2) is presented as a superposition of the fields in two sub-problems. The first problem is solved under purely mechanical boundary conditions and the second problem is solved under purely electrical boundary conditions.

For the purely mechanical problem:

$$u=-\frac{2wH^*}{\pi}\sum_{j=1}^{3}\left[N_j^*C_1^*+L_j^*C_2^*\right]\frac{ae^{i\phi}}{\rho}\left[1-\frac{(a^2-l_{1j}^2)^{1/2}}{a}\right],$$
$$u_z=-\frac{2wH^*}{\pi}\sum_{j=1}^{3}\frac{m_j^*}{\gamma_j^*}\left[N_j^*C_1^*+L_j^*C_2^*\right]\arcsin\left(\frac{a}{l_{2j}}\right), \tag{A.10}$$
$$\psi=-\frac{2wH^*}{\pi}\sum_{j=1}^{3}\frac{k_j^*}{\gamma_j^*}\left[N_j^*C_1^*+L_j^*C_2^*\right]\arcsin\left(\frac{a}{l_{2j}}\right)$$

For $z=0$ and $\rho\prec a$ the following holds:

$$\sigma_{zz}(\rho,0)=-\frac{C_1^*w}{\pi^2(a^2-\rho^2)^{1/2}},$$
$$D_z(\rho,0)=\frac{C_2^*w}{\pi^2(a^2-\rho^2)^{1/2}} \tag{A.11}$$

For the purely electrical problem:

$$u=-\frac{2\psi_0H^*}{\pi}\sum_{j=1}^{3}\left[N_j^*C_3^*+L_j^*C_4^*\right]\frac{ae^{i\phi}}{\rho}\left[1-\frac{\left(a^2-l_{1j}^2\right)^{1/2}}{a}\right],$$
$$u_z=-\frac{2\psi_0H^*}{\pi}\sum_{j=1}^{3}\frac{m_j^*}{\gamma_j^*}\left[N_j^*C_3^*+L_j^*C_4^*\right]\arcsin\left(\frac{a}{l_{2j}}\right), \tag{A.12}$$
$$\psi=-\frac{2\psi_0H^*}{\pi}\sum_{j=1}^{3}\frac{k_j^*}{\gamma_j^*}\left[N_j^*C_3^*+L_j^*C_4^*\right]\arcsin\left(\frac{a}{l_{2j}}\right)$$

For $z = 0$ and $\rho \prec a$ it can be shown that:

$$\sigma_{zz}(\rho,0) = -\frac{C_3^*\psi_0}{\pi^2(a^2-\rho^2)^{1/2}},$$
$$D_z(\rho,0) = \frac{C_4^*\psi_0}{\pi^2(a^2-\rho^2)^{1/2}}. \tag{A.13}$$

We integrate the previous normal stress and electric displacement (Eqs. (A.11) and (A.13)), at $z = 0$ over the contact area:

$$P = -2\pi\int_0^a \sigma_{zz}(\rho,0)\rho d\rho,$$
$$Q = 2\pi\int_0^a D_z(\rho,0)\rho d\rho. \tag{A.14}$$

We finally obtain:

$$P = \frac{2aC_1^*w}{\pi} + \frac{2aC_3^*\psi_0}{\pi},$$
$$Q = \frac{2aC_2^*w}{\pi} + \frac{2aC_4^*\psi_0}{\pi}. \tag{A.15}$$

The previous expressions inter-relate applied concentrated force P, concentrated charge Q, indentation depth w and tip potential ψ_0.

Appendix B

The solutions for the inner system under the inner boundary conditions are:

For purely mechanical problem:

$$u_x^{inner} = -sign(\xi)\frac{w}{\pi^2 a}F_1(z)\cos(\phi)\sqrt{\frac{\left(C_{44}a_{11}+d_{15}^2\right)}{C_{11}C_{44}}}e^{-A^i|\xi|} + F_2(z,\phi),$$
$$u_y^{inner} = -sign(\xi)\frac{w}{\pi^2 a}F_1(z)\sin(\phi)\sqrt{\frac{\left(C_{44}a_{11}+d_{15}^2\right)}{C_{11}C_{44}}}e^{-A^i|\xi|} + F_3(z,\phi),$$
$$u_z^{inner} = -\frac{w}{\pi^2 a}\frac{d_{15}}{C_{44}}F_1(z)e^{-A^i|\xi|} + F_4(z),$$
$$\psi^{inner} = \frac{w}{\pi^2 a}F_1(z)e^{-A^i|\xi|} + F_5(z) \tag{B.1}$$

For purely electrical problem:

$$u_x^{inner} = -sign(\xi)\frac{\psi_0}{\pi^2 a}F_6(z)\cos(\phi)\sqrt{\frac{(C_{44}a_{11}+d_{15}^2)}{C_{11}C_{44}}}e^{-A^i|\xi|} + F_7(z,\phi),$$
$$u_y^{inner} = -sign(\xi)\frac{\psi_0}{\pi^2 a}F_6(z)\sin(\phi)\sqrt{\frac{\left(C_{44}a_{11}+d_{15}^2\right)}{C_{11}C_{44}}}e^{-A^i|\xi|} + F_8(z,\phi),$$
$$u_z^{inner} = -\frac{\psi_0}{\pi^2 a}\frac{d_{15}}{C_{44}}F_6(z)e^{-A^i|\xi|} + F_9(z,\phi),$$
$$\psi^{inner} = \frac{\psi_0}{\pi^2 a}F_6(z)e^{-A^i|\xi|} + F_{10}(z,\phi), \tag{B.2}$$

where $F_i(z,\phi)$, $(i = 2,3,7,8)$ and $F_i(z)$, $(i = 4,5,9,10)$ are functions determined by satisfying (14). $F_1(z)$ and $F_6(z)$ are functions that we are not able to express explicitly but satisfy the normal displacement and potential boundary conditions in (12) and (13): $F_1(0) = 0$ and $F_6(0) = 0$. Remaining boundary conditions related to stress τ_z^{inner} and σ_{zz}^{inner} and electric displacement D_z^{inner} are satisfied to the first leading order.

$F_i(z,\phi)$ $,(i = 2,3,7,8)$ and $F_i(z)$, $(i = 4,5,9,10)$ are defined as follow :

$$F_2(z,\phi) = -\frac{2wH^*}{\pi}\cos(\phi)\sum_{j=1}^{3}\left[N_j^*C_1^* + L_j^*C_2^*\right] \times\left[1-\frac{\left(4a^2-\left(\sqrt{4a^2+z_j^2}-z_j\right)^2\right)}{2a}\right]^{1/2},$$
$$F_3(z,\phi) = -\frac{2wH^*}{\pi}\sin(\phi)\sum_{j=1}^{3}\left[N_j^*C_1^* + L_j^*C_2^*\right] \times\left[1-\frac{\left(4a^2-\left(\sqrt{4a^2+z_j^2}-z_j\right)^2\right)}{2a}\right]^{1/2},$$
$$F_4(z) = -\frac{2wH^*}{\pi}\sum_{j=1}^{3}\frac{m_j^*}{\gamma_j^*}\left(N_j^*C_1^* + L_j^*C_2^*\right)\arcsin\left(\frac{2a}{\sqrt{4a^2+z_j^2}+z_j}\right),$$
$$F_5(z) = -\frac{2wH^*}{\pi}\sum_{j=1}^{3}\frac{k_j^*}{\gamma_j^*}\left(N_j^*C_1^* + L_j^*C_2^*\right)\arcsin\left(\frac{2a}{\sqrt{4a^2+z_j^2}+z_j}\right),$$
$$F_7(z,\phi) = -\frac{2\psi_0H^*}{\pi}\cos(\phi)\sum_{j=1}^{3}\left[N_j^*C_3^* + L_j^*C_4^*\right] \times\left[1-\frac{\left(4a^2-\left(\sqrt{4a^2+z_j^2}-z_j\right)^2\right)}{2a}\right]^{1/2},$$
$$F_8(z,\phi) = -\frac{2\psi_0H^*}{\pi}\sin(\phi)\sum_{j=1}^{3}\left[N_j^*C_3^* + L_j^*C_4^*\right] \times\left[1-\frac{\left(4a^2-\left(\sqrt{4a^2+z_j^2}-z_j\right)^2\right)}{2a}\right]^{1/2},$$
$$F_9(z) = -\frac{2\psi_0H^*}{\pi}\sum_{j=1}^{3}\frac{m_j^*}{\gamma_j^*}\left(N_j^*C_3^* + L_j^*C_4^*\right)\arcsin\left(\frac{2a}{\sqrt{4a^2+z_j^2}+z_j}\right),$$
$$F_{10}(z) = -\frac{2\psi_0H^*}{\pi}\sum_{j=1}^{3}\frac{k_j^*}{\gamma_j^*}\left(N_j^*C_3^* + L_j^*C_4^*\right)\arcsin\left(\frac{2a}{\sqrt{4a^2+z_j^2}+z_j}\right) \tag{B.3}$$

and

$$A^i = \frac{1}{d^*}\sqrt{\frac{C_{11}(d_{15}^2+C_{44}a_{11})}{C_{44}}}. \tag{B.4}$$

Appendix C

We denote $F_1'(0) = \alpha^{flex}, F_6'(0) = \beta^{flex}$. Both α^{flex} and β^{flex} are essentially integration constants and their determination is not something that appears to be possible within the scope of perturbation approach. Their estimation is discussed in Appendix D.

Then, constants f_1^*, f_2^*, f_3^* and f_4^* introduced in (18) and (19) have the following expressions:

$$f_1^* = \alpha^{flex}\frac{(C_{44}d_{33}-C_{33}d_{15})}{C_{44}},\quad f_2^* = \alpha^{flex}\frac{(d_{15}d_{33}+C_{44}a_{33})}{C_{44}},$$
$$f_3^* = \beta^{flex}\frac{(C_{44}d_{33}-C_{33}d_{15})}{C_{44}},\quad f_4^* = \beta^{flex}\frac{(d_{15}d_{33}+C_{44}a_{33})}{C_{44}} \tag{C.1}$$

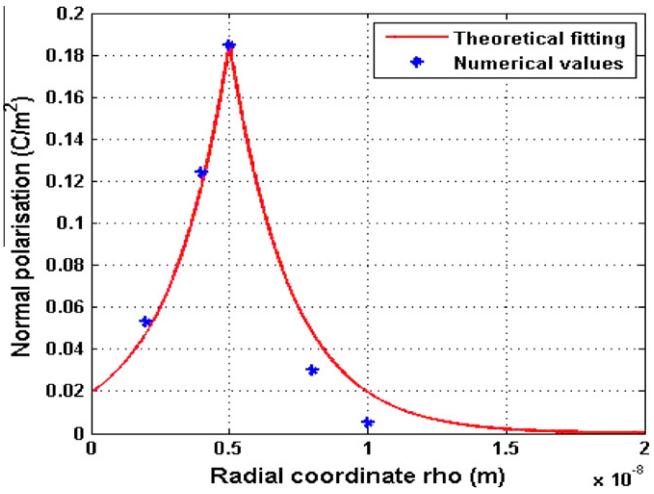

Fig. 4. Variation of the normal polarization for variable radial parameter ρ for $BaTiO_3$.

For our calculations, we use the following elastic stiffness coefficients, piezoelectric coefficients and dielectric permeabilities for $BaTiO_3$ (Giannakopoulos and Suresh, 1999):

Parameter	C_{11}	C_{33}	C_{44}	C_{12}	C_{13}	d_{31}	d_{33}	d_{15}	a_{11}	a_{33}
$BaTiO_3$	166.0	162.0	42.9	76.6	77.5	−4.4	18.6	11.6	11.1	12.5

where C_{ij} in (GPa), d_{ij} in (C/m^2) and a_{ij} in 10^{-9} (F/m). Then, we obtain

$$d^* = 11.5333\ C/m^2 \quad \text{and} \quad A^i_{BT} = 4.2226. \tag{C.2}$$

Appendix D

In order to estimate α^{flex} and consequently f_1^* for the case of Barium Titanate, a numerical calculation was performed using FEMLAB software. A 2D punch problem is solved taking into account flexoelectricity. For this particular simulation, we set the piezoelectric constants to zero since estimation of α^{flex} should be unaffected by this. Plotting normal polarization obtained via the FEM model and via theoretical work, we obtain Fig. 4.

It is shown from Fig. 4 that our theoretical results are in a very good agreement with those found based on the numerical FEM model when taking $\alpha^{flex} \approx 4 \times 10^9$ N/C. Now based on (C.1) relations, we find that $f^*_{1BT} \approx -9 \times 10^{11}$ N/m².

References

Catalan, G., Sinnamon, L.J., Gregg, J.M., 2004. The effect of flexoelectricity on the dielectric properties of inhomogeneously strained ferroelectric thin films. Journal of Physics: Condensed Matter 16 (13), 2253–2264.

Cross, L.E., 2006. Flexoelectric effects: charge separation in insulating solids subjected to elastic strain gradients. Journal Of Materials Science 41, 53–63.

Damjanovic, D., 2005. Contributions to the piezoelectric effect in ferroelectric single crystals and ceramics. Journal of the American Ceramic Society 88 (10), 2663–2676.

Dumitrica, T., Landis, C.M., Yakobson, B.I., 2002. Curvature-induced polarization in carbon nanoshells. Chemical Physics Letters 360 (1–2), 182–188.

Eliseev, E.A., Morozovska, A.N., 2009. General approach for the description of size effects in ferroelectric nanosystems. Journal of Materials Science 44 (19), 5149.

Eliseev, E.A., Morozovska, A.N., Glinchuk, M.D., Blinc, R., 2009. Spontaneous flexoelectric/flexomagnetic effect in nanoferroics. Physical Review B 79, 165433.

Fousek, J., Cross, L.E., Litvin, D.B., 1999. Possible piezoelectric composites based on the flexoelectric effect. Materials Letters 39, 287.

Fu, J.Y., Zhu, W., Li, N., Cross, L.E., 2006. Experimental studies of the converse flexoelectric effect induced by inhomogeneous electric field in a barium strontium titanate composition. Journal of Applied Physics 100, 024112.

Fu, John Y., Zhu, Wenyi, Li, Nan, Smith, Nadine B., Eric Cross, L., 2007. Gradient scaling phenomenon in microsize flexoelectric piezoelectric composites. Applied Physics Letters 91, 182910.

Gharbi, M., Sun, Z.H., Sharma, P., White, K., 2009. The origins of electromechanical indentation size effect in ferroelectrics. Applied Physics Letters 95, 142901.

Giannakopoulos, A.E., Suresh, S., 1999. Theory of indentation of piezoelectric materials. Acta Material 47 (7), 2153–2164.

Hay, J.L., Pharr, G.M., 2000. Instrumented Indentation Testing. In: Kuhn, H., Medlin, D. (Eds.), ASM Handbook, tenth ed., Mechanical Testing and Evaluation, vol. 8 ASM International, Materials Park, OH, USA, pp. 231–242.

Holmes, M.H., 1995. Introduction to Perturbation Methods. Springer-Verlag, New York.

Hong, J., Catalan, G., Scott, J.F., Artacho, E., 2010. The flexoelectricity of barium and strontium titanates from first principles. Journal of Physics: Condensed Matter 22, 112201.

Kalinin, S.V., Meunier, V., 2008. Electronic flexoelectricity in low-dimensional systems. Physical Review B 77 (3), 033403-1-4.

Kalinin, S.V., Karapetian, E., Kachanov, M., 2004. Nanoelectromechanics of piezoresponse force microscopy. Physical Review B 70, 184101.

Karapetian, E., Kachanov, M., Sevostianov, I., 2002. The principle of correspondence between elastic and piezoelectric problems. Archive of Applied Mechanics 72, 564.

Karapetian, E., Kachanov, M., kalinin, S.V., 2005. Nanoelectromechanics of piezoelectric indentation and applications to scanning probe microscopies of ferroelectric materials. Philosophical Magazine 85, 1017–1051.

Ma, W., Cross, L.E., 2001. Large flexoelectric polarization in ceramic lead magnesium niobate. Applied Physics Letters 79 (19), 4420–4422.

Ma, W., Cross, L.E., 2002. Flexoelectric polarization in barium strontium titanate in the paraelectric state. Applied Physics Letters 81 (19), 3440–3442.

Ma, W., Cross, L.E., 2003. Strain-gradient induced electric polarization in lead zirconate titanate ceramics. Applied Physics Letters 82 (19), 3923–3925.

Ma, W., Cross, L.E., 2006. Flexoelectricity of barium titanate. Applied Physics Letters 88, 232902.

Majdoub, M.S., Sharma, P., Cagin, T., 2008a. Enhanced size-dependent piezoelectricity and elasticity in nanostructures due to the flexoelectric effect. Physical Review B 77, 125424-1–125424-9.

Majdoub, M.S., Sharma, P., Cagin, T., 2008b. Dramatic enhancement in energy harvesting for a narrow range of dimensions in piezoelectric nanostructures. Physical Review B 78, 121407(R).

Majdoub, M.S., Maranganti, R., Sharma, P., 2009a. Understanding the origins of the intrinsic dead layer effect in nanocapacitors. Physical Review B 79, 115412.

Majdoub, M.S., Sharma, P., Cagin, T., 2009b. Physical Review B 79, 119904(E).

Majdoub, M.S., Sharma, P., Cagin, T., 2009c. Physical Review B 79, 159901(E).

Oliver, W.C., Pharr, G.M., 1992. An improved technique for determining hardness and elastic modulus using load and displacement sensing indentation experiments. Journal of Materials Research 7, 1564.

Maranganti, R., Sharma, P., 2009. Atomistic determination of flexoelectric properties of crystalline dielectrics. Physical Review B 80, 054109.

Sun, Z.H., White, K.W., 2008. Nanoindentation-induced plastic deformation and fracture behavior difference between a- and c-domains of BaTiO3 single crystal. Journal of Applied Physics 104, 103506.

Tagantsev, A.K., 1986. Piezoelectricity and flexoelectricity in crystalline dielectrics. Physical Review B 34, 5883–5889.

Tagantsev, A.K., 1991. Electric polarization in crystals and its response to thermal and elastic perturbations. Phase Transitions 35, 119–203.

Tagantsev, A.K., Meunier, V., Sharma, P., 2009. Novel electromechanical phenomena at the nanoscale: phenomenological theory and atomistic modeling. MRS Bulletin 34 (9), 643–647.

Zubko, P., Catalan, G., Buckley, A., Welche, P.R.L., Scott, J.F., 2007. Strain-gradient induced polarization in $SrTiO_3$. Physical Review Letters 99, 167601.